JOURNAL OF MATERIALS SCIENCE 18 (1983) 3128–3136

A new statistical model of the hydrogen embrittlement of steel

T. H. GRUNDY, T. J. DAVIES, D. A. RYDER
Department of Metallurgy, University of Manchester/UMIST, Metallurgy Building, Grosvenor Street, Manchester, UK

The hydrogen embrittlement of a hardened and tempered plain carbon, eutectoid steel of 1930 MN m^{-2} tensile strength has been studied. Plain, unnotched specimens were electrolytically charged with hydrogen and then subjected to tensile tests and delayed failure tests at constant load. The test results showed a scatter characteristic of a stochastic process and it is shown that the distribution can be described by a modified form of the Weibull probability function. Fractographic results are reported which show that fracture initiated internally at oxide inclusions and it is suggested that the embrittlement can be explained by a pressure mechanism.

Nomenclature

P_F	Probability of fracture.
P_s	Probability of survival = $(1 - P_F)$.
σ_0	Weibull equation scale factor (MN m^{-2}).
σ_F	Fracture stress, load at fracture divided by original cross-sectional area (MN m^{-2}).
m	Weibull equation modulus.
n_T, n_D	The cumulative number of specimens failed up to the class interval of interest (tensile test n_T, delayed failure n_D).
N	Total number of tests performed = 40.
K	Delayed failure constant (sec^{-1}).
t_F	time to failure at constant stress (sec).
t_0	Modified Weibull equation time constant = 1 sec.
T, T_F, T_Y	T, time in tensile test, T_Y, time to reach elastic limit, T_F, time to reach fracture stress (sec).
V_F, V_0	Specimen volume terms to describe size effect in Weibull equation.
x, k, l, y, A	Various constants defined when used.

1. Introduction

Small quantities of hydrogen can seriously reduce the load bearing properties of steel and the ease of hydrogen pick-up during manufacture or service life of components has resulted in a large research effort to understand the phenomenon. Attempts to quantify the effects of hydrogen on strength and ductility have been bedevilled by the scatter in results; consequently most recent researchers have concentrated on the effect of hydrogen on fracture toughness. However statistical interpretation of mechanical property scatter has been successfully developed to provide a means of interpreting the brittle behaviour of ceramic materials. It seemed reasonable therefore to attempt to examine how far the properties of embrittled steel could be described using suitably modified forms of the statistical expressions for ceramic materials; this is discussed below.

2. Experimental details

To enable full use to be made of statistical analyses large numbers of simple specimens are required and with this in mind a high quality spring steel wire was used (0.81% C, 0.70% Mn, 0.16% Si, 0.007% P, 0.01% S of 2 mm diameter having a specification similar to BS 5216M). To ensure a high susceptibility to hydrogen embrittlement (HE) the wire was heat treated to give a tempered martensite structure of 1930 MN m^{-2} tensile

0022–2461/83 $03.00 + .12

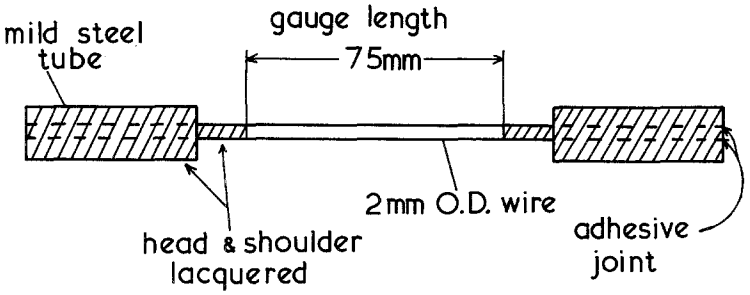

Figure 1 Specimen design.

strength. Because the number of test pieces was large the test piece design was correspondingly simple. 150 mm lengths of heat treated wire were glued into pieces of mild steel tube (using "Loctite", engineering adhesive) which thus formed the heads of the specimens which were gripped by the testing machines (see Fig. 1).

The specimens were protectively lacquered (see Fig. 1) to ensure that only the gauge length was exposed to hydrogen charging. Prior to hydrogen charging each specimen gauge length was polished to a 25 μm diamond finish, etched for 15 sec in 2% Nital and then dried.

Specimens were cathodically charged with hydrogen for 3 min at 1 A m^{-2} current density in 0.4 M sulphuric acid solution poisoned with 5 mg l^{-1} of arsenious trioxide. All mechanical tests commenced 5 min after charging to ensure comparability of results. (Other results [1] not reported here indicated that no significant outgassing occurred during any of the tests reported).

The effect of hydrogen was assessed by two tensile properties.

1. The tensile strength, determined from tests at constant crosshead speed of 1 mm min^{-1} in an Instron Universal testing machine with a 10 000 kg load cell; forty specimens were tested.

2. The times to failure at constant load (i.e. delayed failure or static fatigue) were measured for forty specimens each at applied stresses of 1880, 1850, 1820 and 1790 MN m^{-2} in a dead weight loaded single lever machine with a mechanical advantage of 20 : 1.

Fractured specimens were stored in a vacuum dessicator and examined fractographically using a scanning electron microscope.

3. Results

The values of the tensile strength of the 40 specimens tested are listed in Table I (values quoted are load at fracture divided by the original cross-sectional area); the reduction in cross-section (% RA) was typically 6%. Unhydrogenated specimens had an average tensile strength of 1930 MN m^{-2} with about 45% RA and fracture was by microvoid coalescence. Examination of the embrittled fracture surfaces showed that fracture originated at near-spherical oxide inclusions inside the steel and the fracture mode of the matrix was mainly intergranular. Energy dispersive X-ray analysis indicated that the inclusions were mainly composed of mixed calcium, silicon and aluminium oxides but occasionally traces of magnesium oxide, iron oxide and manganese sulphide were detected. Typically these inclusions were ~ 20 μm diameter and located ~ 50 μm below the surface of the wire specimens. Examples of the fracture surface and origin of fracture are shown in Figs. 2 and 3. The times to failure of specimens held at constant load are listed in Tables II to V for each of the test stresses. To allow completion of the experiments in a reasonable time any test that did not produce a result after 2 h was terminated and such results are marked NF in the tables. Fractography again showed that fracture was initiated by oxide inclusions, and grew in a brittle intergrannular manner; typical examples of fracture surfaces and fracture origins are shown in Figs. 4 and 5.

TABLE I 40 values of embrittled tensile strength, σ_F (MN m^{-2})

1897,	1842,	1897,	1942,	1897,	1937,	1848,	1888,
1891,	1915,	1879,	1939,	1912,	1929,	1879,	1903,
1899,	1882,	1920,	1876,	1912,	1937,	1915,	1909,
1882,	1937,	1939,	1866,	1879,	1854,	1922,	1911,
1873,	1931,	1924,	1900,	1880,	1860,	1928,	1854.

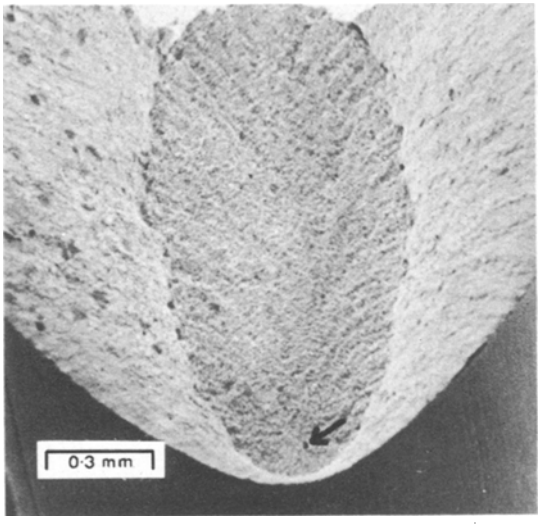

Figure 2 SEM fractograph. Rising stress test.

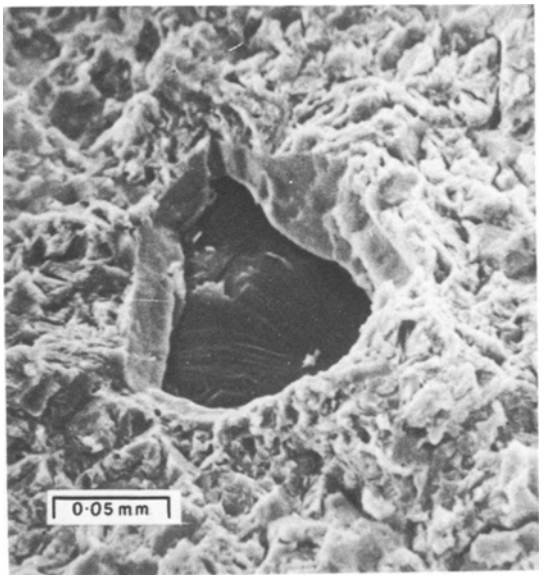

Figure 3 SEM fractograph. Rising stress test.

4. Statistical analysis

4.1. Fracture strength

The fracture strength of ceramic materials is frequently modelled by an expression of the Weibull [2] type, i.e.:

$$(1 - P_F) = \exp\left[-\left(\frac{\sigma_F - \sigma_u}{\sigma_0}\right)^m\right] \quad (1)$$

where at a fracture strength σ_F there is a probability of fracture P_F, σ_u is the stress below which $P_F = 0$ (usually taken as zero), σ_0 is a scale factor and m is the Weibull modulus.

To fit the fracture strength results of Table I to a Weibull equation the strengths were grouped into classes (1840 to 1849, 1850 to 1859, etc.) and a probability of fracture assigned to each class according to:

$$P_F = n_T/(N + 1) \quad (2)$$

where n_T is the number of specimens which fractured up to and including the class interval of interest and N is the total number of tests (40 in this case). The fracture stress corresponding to that P_F is taken as the middle value of the class in question, e.g. for 1840 to 1849 $\sigma_F = 1845\,\mathrm{MN\,m^{-2}}$.

Using linear regression the following straight line was fitted to the pairs of σ_F, P_F values determined and gave the results given in Table VI and shown graphically in Fig. 6.

$$\ln \ln [1/(1 - P_F)] = 77.97 \ln (\sigma_F) - 589.0 \quad (3a)$$

or

$$(1 - P_F) = \exp\left[-\left(\frac{\sigma_F}{1909}\right)^{77.97}\right]. \quad (3b)$$

The usual statistical tests showed that the fitted equation was a good representation of the results (see [1]).

4.2. Delayed failure

Yokobori [3] demonstrated that the delayed failure of glass was a stochastic process analogous to the radioactive decay of nuclei. Examination of the delayed failure results presented here also shows an exponential distribution of failure times. Graphically this is displayed in Figs. 7, 8, 9 and 10 where the failure times (from Tables II to V) for each of the applied stresses are grouped into classes (1 to 50, 51 to 100 sec, etc.) and the probability of survival, P_s computed from:

$$P_s = 1 - [n_D/(N + 1)] \quad (4)$$

TABLE II 40 values of times to failure (sec) at 1880 $\mathrm{MN\,m^{-2}}$ applied stress

25,	6,	143,	3,	8,	11,	37,	92,
62,	137,	4,	10,	199,	31,	75,	214,
27,	8,	5,	27,	97,	72,	45,	124,
294,	6,	119,	127,	11,	141,	176,	5,
10,	20,	5,	242,	5,	16,	5,	8.

TABLE III 40 values times to failure (sec) at 1850 MN m^{-2} applied stress

120,	811,	311,	104,	219,	166,	44,	353,
76,	81,	88,	61,	115,	156,	324,	78,
54,	100,	58,	171,	449,	876,	97,	142,
94,	102,	128,	236,	196,	122,	299,	260,
66,	420,	580,	179,	336,	24,	57,	370.

where n_D is the number of specimens which failed up to and including the class interval of interest and N is the total number of tests ($N = 40$ at each of the stress levels). The t_F corresponding to a given P_s is the value at the end of the class interval of interest, e.g. for 1 to 50, $t_F = 50$).

Quantitatively the relation between P_s and t_F can be expressed as:

$$\ln (P_s) = -Kt_F \tag{5}$$

where K is a constant dependent upon the applied stress. Using regression analysis straight lines were fitted to each of the graphs in Figs. 7 to 10. Checks again showed the lines were a reasonable representation of the data, the slight deviation visible at 1790 MN m^{-2} (Fig. 10) is not considered significant (see [1]).

The variation of the delayed failure constant, K, and the applied stress is shown in Table VII and a logarithmic plot of K against σ_F shown in Fig. 11 again demonstrates a linear correlation. Regression analysis yields

$$\ln (K) = 64.40 \ln (\sigma_F) - 490.0. \tag{6}$$

Combination of Equations 5 and 6 to eliminate the constant K gives:

$$\ln \ln (1/P_s) = 64.40 \ln (\sigma_F) + \ln (t_F) - 490.0 \tag{7a}$$

or

$$P_s = (1 - P_F) = \exp\left[-\left(\frac{t_F}{t_0}\right)\left(\frac{\sigma_F}{2016}\right)^{64.40}\right] \tag{7b}$$

where $t_0 = 1$.

A striking similarity evident between Equations 7a and 7b and the Weibull Equations 3a and 3b developed in the previous section is considered in the next section.

4.3. A combined expression to cover delayed failure and rising stress fracture strength

The question of strength–probability–time relationships has already been considered for ceramics by Davidge *et al.* [4] and a parallel approach to this is outlined below.

To develop such a combined expression it is necessary to develop a time factor for the rising stress test. Clearly this will be some function of the crosshead speed (more correctly strain rate) and one can intuitively see that such a term is relevant from the well known strain rate sensitivity of hydrogen embrittlement [5]. In this context, to develop a combined equation, an "equivalent time to failure" for specimens fracturing in a rising stress test is required. By "equivalent time to failure" is meant the time t_F for a specimen breaking at stress σ_F in a rising stress test; this is equal to the time a specimen would have survived at the same but constant stress, σ_F (i.e. in delayed failure). Thus there will be a different equivalent time to failure for each specimen even when they are all tested at the same crosshead speed because they all reach different stresses (loads) before breaking. This equivalent time to failure (t_F) is not simply the real time taken during a test (T_F) to reach the fracture stress but is related to it by:

$$\int_0^{T_F} \frac{dT}{t_F} = 1. \tag{8}$$

This integral implies that the rising stress can be divided into an infinite number of constant stress (delayed failure) steps with each of which is associated a fraction ($\delta T/t_F$) of the total time to failure and that the sum of these parts is unity. Equation 8 can be reorganized to find the relation between the measurable real time, T_F, and the

TABLE IV 40 values times to failure (sec) at 1820 MN m^{-2} applied stress

583,	183,	22,	123,	3262,	29,	144,	322,
640,	57,	163,	1506,	6,	136,	392,	540,
2015,	304,	1219,	469,	316,	633,	133,	692,
1458,	302,	236,	197,	220,	54,	618,	7,
495,	201,	428,	21,	418,	2479,	852,	387.

TABLE V 40 values times to failure (sec) at 1790 MN m^{-2} applied stress

339,	2287,	NF*,	39,	NF,	1092,	305,	228,
1849,	1009,	NF,	130,	2166,	212,	383,	264,
5,	724,	1853,	144,	330,	482,	299,	NF,
2514,	NF,	291,	357,	170,	448,	NF,	19,
806,	1021,	294,	484,	411,	336,	3347,	NF,

*NF means no failure after 7200 sec on load.

equivalent time, t_F, by assuming that the embrittlement is greatest at the high stresses and that quantitatively this is defined by the delayed failure equation (Equation 7), i.e. writing this as:

$$t\sigma^x = A \tag{9}$$

where $x = 64.40$ and $A = 2016^{64.40} \ln (1/P_s)$. The fraction of the specimen life (dT/t_F) spent at stress, σ, is $[(\sigma^x dT)/A]$ so that Equation 8 becomes:

$$1 = \int_0^{T_F} \frac{\sigma^x}{A} \, dT. \tag{10}$$

The relation between the stress, σ, and the time taken to reach that stress, T, can be found by re-examining the load–time curve shown in Fig. 12 and is specified as:

$$\text{Elastic range} \qquad \sigma = kT \qquad \text{for } 0 < T < T_E \tag{11a}$$

$$\text{Plastic range} \qquad \sigma = lT^{1/y} \qquad \text{for } T_E < T < T_F \tag{11b}$$

where k and l are constants and $y = 11.01$ (determined from a logarithmic plot of σ against T using data from Fig. 12, as shown in [1]).

Using Equations 11a and 11b it is possible to substitute for the stress, σ, and Equation 10 yields:

$$1 = k^x \int_0^{T_E} \frac{T^x}{A} \, dT + l^x \int_0^{T_F} \frac{T^{x/y}}{A} \, dT. \tag{12}$$

After integration and rearrangement of Equation 12 and use of $t_F \sigma_F^x = A$ from Equation 9, this reduces to:

$$t_F = \frac{T_F}{[(x/y) + 1]} - T_E \left(\frac{\sigma_E}{\sigma_F}\right)^x \left[\frac{x(y-1)}{(x+y)(x+1)}\right] \tag{13}$$

where σ_E corresponds to the T_E of Equation 11a.

For the particular values of σ_F and x encountered in this work Equation 13 simplifies to:

$$t_F = \frac{T_F}{[(x/y + 1]} = \frac{T_F}{6.85}. \tag{14}$$

A comparison of the values of the equivalent

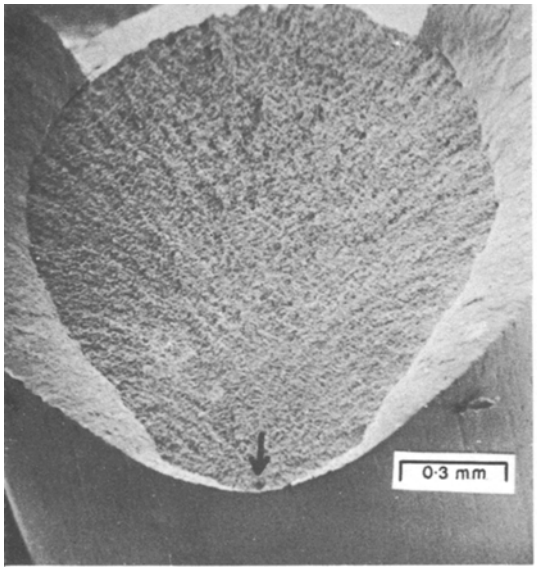

Figure 4 SEM fractograph. Delayed fracture test.

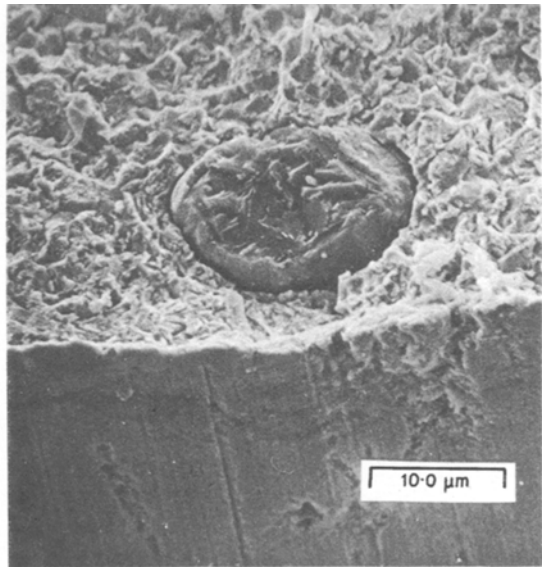

Figure 5 SEM fractograph. Delayed fracture test.

TABLE VI Tensile test parameters

Fracture stress σ_F (MN m^{-2})	Probability of fracture P_F	Time to reach σ_F, T_F	Equivalent time to failure, t_F (sec)	
			From Equation 14	From Equation 7a
1845	0.0488	171	25.1	20.4
1855	0.0976	176	25.8	22.0
1865	0.146	185	27.1	23.7
1875	0.268	196	28.7	25.4
1885	0.366	209	30.7	27.3
1895	0.488	220	32.3	29.4
1905	0.561	233	34.2	31.5
1915	0.683	246	36.1	33.9
1925	0.805	263	38.6	36.4
1935	0.951	278	40.8	39.0
1945	0.976	300	44.0	41.8

time to failure t_F calculated from the delayed failure results (Equation 7a) and from the rising stress time data (Equation 14), shown in Table VI, reveals them to be identical within experimental error. In other words Equation 7b

$$P_s = (1 - P_F) = \exp\left[-\left(\frac{t_F}{1}\right)\left(\frac{\sigma_F}{2016}\right)^{64.40}\right] \quad (15)$$

gives the probability–time–strength relationship for both delayed failure (where t_F is the time to failure at a given applied stress σ_F and probability P_F) and rising stress tests (where t_F is now the equivalent time to failure, found from Equation 14 from the real time of test, at a given fracture strength, σ_F and probability P_F) for this embrittled steel.

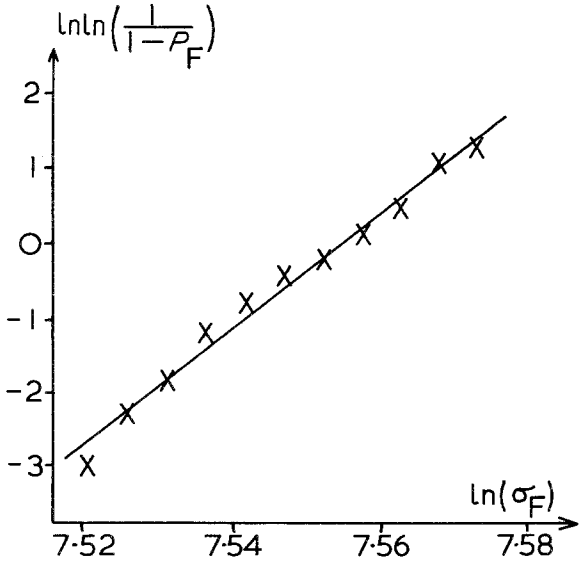

Figure 6 Graph of $\ln\ln(1/1 - P_F)$ against $\ln \sigma_F$ for Table VI.

Strictly speaking the analysis is only valid for tensile tests at constant strain rate but in fact in this case although tests were only conducted at constant crosshead speed the strain rate did not change drastically from initial loading to fracture (see [1]).

5. Discussion

The generalized form of the expression developed above is:

$$\text{Time effect } P_s = (1 - P_F) = \exp\left[-\left(\frac{t_F}{t_0}\right)\left(\frac{\sigma_F}{\sigma_0}\right)^m\right] \quad (16)$$

and is analogous to versions of the Weibull equation which describe size effects in ceramics, namely:

$$\text{Size effect } P_s = (1 - P_F) = \exp\left[-\left(\frac{V_F}{V_0}\right)\left(\frac{\sigma_F}{\sigma_0}\right)^m\right] \quad (17)$$

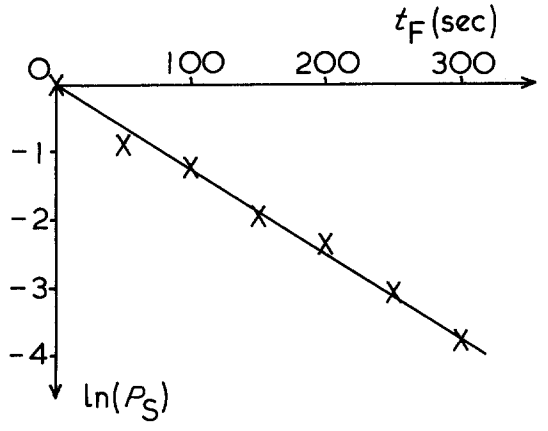

Figure 7 Graph of ln (P_s) against t_F at 1880 MN m^{-2}.

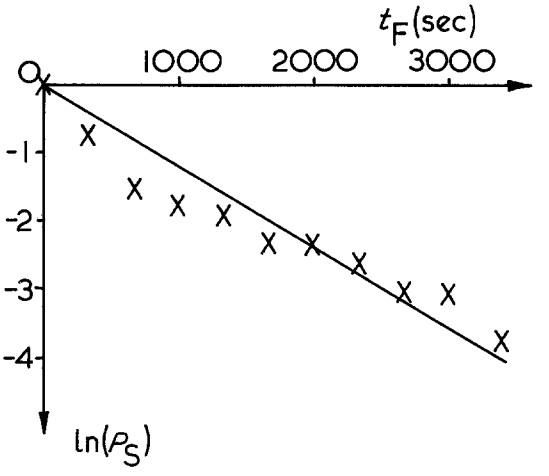

Figure 9 Graph of ln (P_s) against t_F at 1820 MN m^{-2}.

where the stressed specimen volume is V_F (relative to unit volume V_0) and predicts that larger specimens are weaker. The time equation in the same way shows that for delayed failure, long times to failure occur at low applied stresses (for a given P_F) or conversely for rising stress tests that low strain rates (equivalent to large t_F) produce low fracture strengths (for a given P_F). This predicted strain rate effect is of course exactly what has been observed for the hydrogen embrittlement of steel [5]. In fact it is possible that a size effect also exists in hydrogen embrittlement and that a more complete equation would be

$$P_s = (1 - P_F) = \exp\left[-\left(\frac{t_F}{t_0}\right)\left(\frac{V_F}{V_0}\right)\left(\frac{\sigma_F}{\sigma_0}\right)^m\right]. \quad (18)$$

Re-analysis of older experimental work, reported elsewhere [1], supports an expression of the above type. One important feature of the equation is that it mathematically illustrates that delayed failure and rising stress hydrogen embrittlement are two facets of the same effect: this may not be unexpected but it has not been well established by previous work on hydrogen embrittlement.

The applicability of the statistics of brittle fracture to the hydrogen embrittlement of steel is not surprising. The fractography indicated that fracture initiated at oxide inclusions, analogous to internal cracks in a classic brittle material, and that crack growth occurred in one step with no or little subcritical crack growth. This is again analogous to the stress reaching a critical value for catastrophic crack extension in a classic brittle material.

The experimental observation that only oxide inclusions provided suitable crack initiation sites is supported by Ciszewski *et al.* [6] who found that only oxide inclusion (not sulphide) were surrounded by stress fields and/or cracks after quenching and tempering heat treatments in steel;

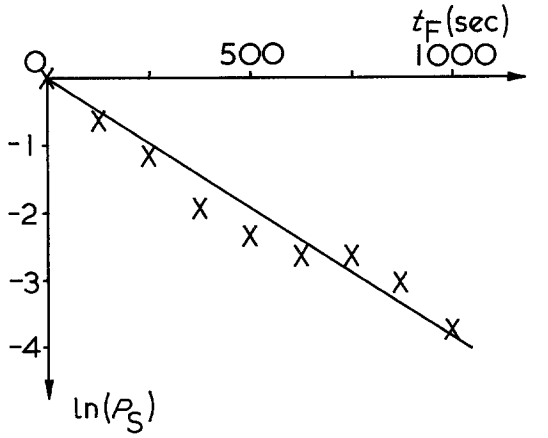

Figure 8 Graph of ln (P_s) against t_F at 1850 MN m^{-2}.

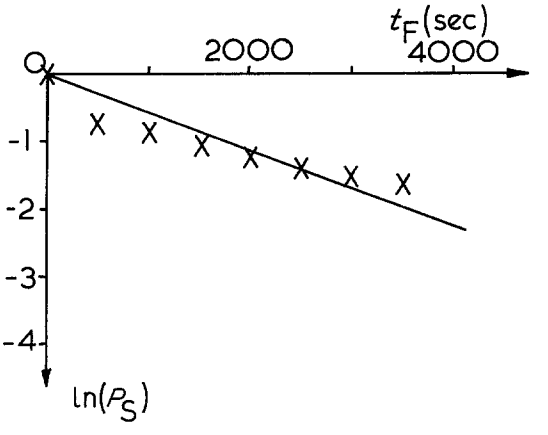

Figure 10 Graph of ln (P_s) against t_F at 1790 MN m^{-2}.

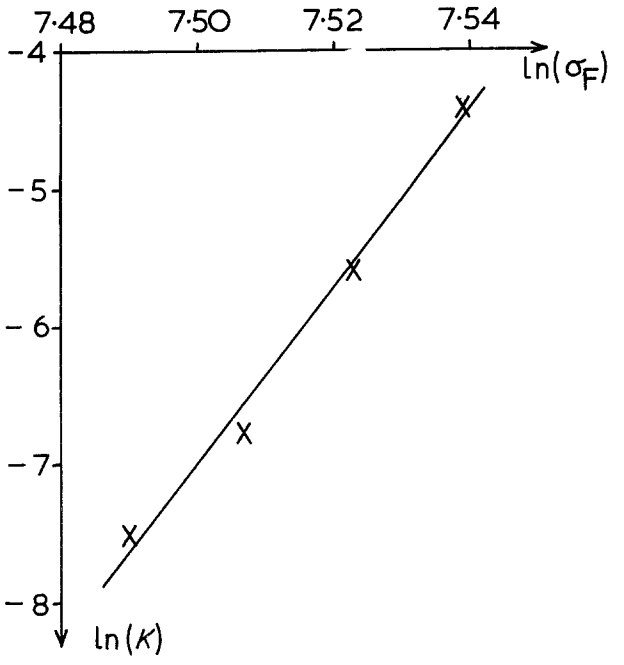

Figure 11 Graph of ln (K) against ln (σ_F) from Table VII.

the presence of these stress fields increased the effects of hydrogen embrittlement in a given steel.

The extent to which the Equations 16 and 17 developed above apply to other cases of hydrogen embrittlement in steel in not unequivocal. One might expect that their application may be limited to the HE of high strength steels where the brittle fracture is characterized macroscopically by a low %RA and by predominantly brittle mode microscopic fracture. The analysis will be less pertinent to the HE of low strength steels where the microscopic fracture mode can be ductile. (It has been shown that HE of low strength steels produces only a change in void size during failure by microvoid coalescence [7]; at the same time the severe loss of ductility is consistent with a macroscopically brittle failure mode.)

In this context it is worth noting that the mechanism of hydrogen embrittlement operating very probably involves hydrogen gas pressure developing at non-deformable oxide inclusions and it is possible therefore that the relationships developed apply only where pressure mechanisms (as detailed by Tetelman [8]) are dominant.

The practical use of strength–probability–time relations in ceramics for design purposes is already

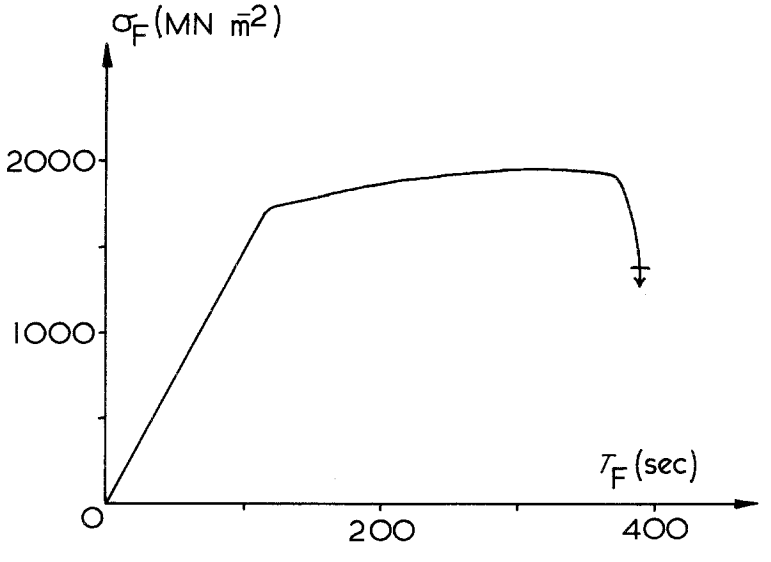

Figure 12 Graph of σ_F against T_F real load–time curve.

TABLE VII Variation of delayed failure constant, K, with applied stress, σ_F

Applied stress, σ_F (MN m^{-2})	Constant, K (sec^{-1})
1880	0.01226
1850	0.003828
1820	0.001162
1790	0.0005466

established and it is possible that the equations proposed in this paper could be put to similar use for steel. Perhaps the application of these ideas in design of products which suffer unavoidable hydrogen embrittlement is limited but such statistical techniques might well be useful for example, in material selection and in ranking materials, microstructures and de-embrittling treatments. One advantage in this respect is that only very simple test pieces and experiments are required to yield quantitative comparisons. Additionally, because this method of testing and analysing HE deals with simply loaded, plain specimens, the HE effects that are observed relate unambiguously to the microstructural state of the material.

6. Conclusions

1. (a) The effect of hydrogen on the tensile properties of a 0.8% C quenched and tempered steel can be described by a probabilistic expression. This is a Weibull equation modified to include a time term, thus:

$$P_s = (1 - P_F) = \exp\left[-\left(\frac{t_F}{t_0}\right)\left(\frac{\sigma_F}{\sigma_0}\right)^m\right].$$

(b) This expression covers both delayed failure and rising stress test embrittlement thus demonstrating their common origin.

2. The mechanism of hydrogen embrittlement in this study is most likely the pressure of molecular hydrogen at defect sites.

3. The defect sites were metallographically identified as oxide inclusions.

References

1. T. H. GRUNDY, PhD thesis, UMIST (1982).
2. W. WEIBULL, *J. Appl. Mech.* 18 (1951) 293.
3. T. YOKOBORI, "The Strength, Fracture and Fatigue on Materials" (P. Noordhoff, The Netherlands, 1965).
4. R. W. DAVIDGE, J. R. McCLAREN and G. TAPPIN, *J. Mater. Sci.* 8.2 (1973) 1699.
5. A. R. TROIANO, *Trans. ASM* 52 (1960) 54.
6. A. CISZEWSKI and T. RADOMSKI, "S.C.C. and H.E. of Iron Base Alloys", edited by R. W. Staehle, J. Hochmann, R. D. McCright and J. E. Slater, 1973 (NACE, Houston, USA, 1977) p. 671.
7. A. W. THOMPSON, *Met. Trans.* 10A (1979) 727.
8. A. S. TETELMAN, "Fracture of Solids" (AIME, Warendale, USA, 1963) p. 671.

Received 25 January
and accepted 24 February 1983